HHS Public Access

Author manuscript

Sci Transl Med. Author manuscript; available in PMC 2024 August 10.

Published in final edited form as:

Sci Transl Med. 2024 May 22; 16(748): eadk1358. doi:10.1126/scitranslmed.adk1358.

Gain-of-function mutations of TRPV4 acting in endothelial cells drive blood-CNS barrier breakdown and motor neuron degeneration in mice

Jeremy M. Sullivan[1,*], **Anna M. Bagnell**[1], **Jonathan Alevy**[2], **Elvia Mena Avila**[3,4], **Ljubica Mihaljević**[5], **Pamela C. Saavedra-Rivera**[1], **Lingling Kong**[1], **Jennifer S. Huh**[1], **Brett A. McCray**[1], **William H. Aisenberg**[1], **Aamir R. Zuberi**[6], **Laurent Bogdanik**[6], **Cathleen M. Lutz**[6], **Zhaozhu Qiu**[2,5], **Katharina A. Quinlan**[3,4], **Peter C. Searson**[7,8,9], **Charlotte J. Sumner**[1,2,*]

[1]Department of Neurology, Johns Hopkins University School of Medicine; Baltimore, MD 21205, USA.

[2]Solomon H. Snyder Department of Neuroscience, Johns Hopkins University School of Medicine; Baltimore, MD 21205, USA.

[3]George and Anne Ryan Institute for Neuroscience, University of Rhode Island; Kingston, RI 02881, USA.

[4]Department of Biomedical and Pharmaceutical Sciences, College of Pharmacy, University of Rhode Island; Kingston, RI 02881, USA.

[5]Department of Physiology, Johns Hopkins University School of Medicine; Baltimore, MD 21205, USA.

[6]The Jackson Laboratory; Bar Harbor, ME 04609, USA.

[7]Institute for Nanobiotechnology, Johns Hopkins University; Baltimore, MD 21218, USA.

[8]Department of Biomedical Engineering, Johns Hopkins University; Baltimore, MD 21218, USA.

[9]Department of Materials Science and Engineering, Johns Hopkins University; Baltimore, MD 21218, USA.

[*]Corresponding authors. Charlotte J. Sumner, csumner1@jhmi.edu, Jeremy M. Sullivan, jsulli45@jhmi.edu.

Author contributions: J.M.S., A.M.B., and C.J.S. conceptualized the study. C.M.L., L.B., and A.R.Z. designed and generated the mouse models. J.M.S. (histology, biochemistry, calcium imaging – primary endothelial cells, mouse motor behavior, GSK219 study), A.M.B. (calcium imaging – primary endothelial cells, immunofluorescence, TEER, mouse motor behavior), J.A. (histology), E.M.A. (spinal cord electrophysiology), L.M. (whole-cell patch clamp electrophysiology), P.C.S.-R. (mouse motor behavior, GSK219 study), L.K. (TEM), J.S.H. (biochemistry, mouse motor behavior), B.A.M. (calcium imaging – MN1 cells, mouse motor behavior), and W.H.A. (mouse motor behavior) performed experiments and analyzed data. C.J.S., Z.Q., P.C.S., K.A.Q., and J.M.S. acquired funding. Z.Q., K.A.Q., P.C.S., and C.J.S. supervised the study. J.M.S. and C.J.S. wrote the original draft of the manuscript, which was then revised with input from all authors.

Competing interests: C.J.S. has been a consultant to Avexis, Novartis, Ionis Pharmaceuticals, Biogen, PTC Therapeutics, Roche, Genentech, Cytokinetics, Sarepta, Nura Bio, Actio Biosciences, Biomarin, Epirium, Scholar Rock, and Atalanta. C.J.S. previously received research grant support from Ionis Pharmaceuticals and Argenx, and currently receives grant support from Roche, Biogen and Actio Biosciences. C.J.S. is a nonpaid advisor to Cure SMA, SMA Europe, Kennedy's Disease Association, CMT Research Foundation, and CMT Association. C.J.S. is a coholder of two pending patent applications (BIOL0274USA and BIOL0293WO) with Ionis Pharmaceuticals on antisense oligonucleotides targeting SMN-AS1. All other authors have no competing interests to declare.

Data and materials availability: All data are available in the main text or the supplementary materials. *Trpv4*^{R269C} (Stock #26714) and *Trpv4*^{R232C} (Stock #30223) knock-in mice are available from The Jackson Laboratory.

Abstract

Blood-CNS barrier disruption is a hallmark of numerous neurological disorders; yet, whether barrier breakdown is sufficient to trigger neurodegenerative disease remains unresolved. Therapeutic strategies to mitigate barrier hyperpermeability are also limited. Dominant missense mutations of the cation channel transient receptor potential vanilloid 4 (TRPV4) cause forms of hereditary motor neuron disease. To gain insights into the cellular basis of these disorders, we generated knock-in mouse models of TRPV4 channelopathy by introducing two disease-causing mutations (R269C, R232C) into the endogenous mouse *Trpv4* gene. TRPV4 mutant mice exhibited weakness, early lethality, and regional motor neuron loss. Genetic deletion of the mutant *Trpv4* allele from endothelial cells (but not neurons, glia, or muscle) rescued these phenotypes. Symptomatic mutant mice exhibited focal disruptions of blood-spinal cord barrier (BSCB) integrity, associated with a gain-of-function of mutant TRPV4 channel activity in neural vascular endothelial cells (NVECs) and alterations of NVEC tight junction structure. Systemic administration of a TRPV4-specific antagonist abrogated channel-mediated BSCB impairments and provided a marked phenotypic rescue of symptomatic mutant mice. Together, our findings show that mutant TRPV4 channels can drive motor neuron degeneration in a non-cell autonomous manner by precipitating focal breakdown of the BSCB. Further, these data highlight the reversibility of TRPV4-mediated BSCB impairments and identify a potential therapeutic strategy for patients with TRPV4 mutations.

INTRODUCTION:

Disruption of blood-CNS barriers has been implicated in the pathogenesis of chronic and acute neurodegenerative disorders, including Alzheimer's disease, amyotrophic lateral sclerosis, multiple sclerosis, traumatic brain and spinal cord injury, stroke, and neuropathic pain after nerve injury (1–4). As with other blood-CNS barriers, the blood-spinal cord barrier (BSCB) tightly regulates the exchange of solutes between blood and nervous tissues, a function critical for neuronal homeostasis. Neural vascular endothelial cells (NVECs) represent a core element of the BSCB by forming specialized intercellular junctional complexes, comprising tight and adherens junctions, that limit paracellular passage of neurotoxic blood components into the spinal cord parenchyma. Nonetheless, the extent to which BSCB impairment is sufficient, in and of itself, to drive neuropathology in disease remains unknown. Furthermore, therapies to limit BSCB hyperpermeability are lacking.

Transient receptor potential vanilloid 4 (TRPV4) is currently the sole ion channel associated with hereditary motor neuron disease. Autosomal dominant (or rarely recessive) missense mutations of this channel cause forms of distal spinal muscular atrophy (dSMA) and Charcot-Marie-Tooth disease type 2 (CMT2) (5–11). These disorders result in weakness of neck, diaphragm, limb, and vocal cord muscles, innervated by spinal cord and brainstem motor neurons. Although patients exhibit variability in age at onset (5, 9–12), phenotypic manifestations, and clinical severity (5, 9–12), early-onset disease with early lethality is not uncommon. Unfortunately, there is currently no treatment for these disorders and no mouse models of TRPV4 channelopathy have yet been described that might enable preclinical therapeutic assessments.

TRPV4 is a broadly expressed, calcium-permeable channel that functions as a homotetramer at the plasma membrane, where it is activated by a variety of environmental and chemical stimuli (13, 14). Structurally, each TRPV4 protomer comprises six transmembrane domains and intracellular N- and C-termini. Motor neuron disease-causing mutations occur primarily on the convex face of a prominent ankyrin repeat domain within the N-terminus (5, 14–17). In heterologous expression systems, mutant TRPV4 channels exhibit elevated channel activity (5, 6, 14, 16, 18), suggesting that TRPV4 antagonism may represent a therapeutic strategy for patients with TRPV4 mutations. It remains unknown, however, whether mutant TRPV4 channels also exhibit altered channel activity when expressed endogenously and how this altered function precipitates motor neuron degeneration in vivo. The goal of this study was to interrogate the cellular basis of TRPV4-mediated neurodegenerative disease by generating and characterizing knock-in mouse models expressing human disease-causing TRPV4 mutations. Here, we show that mutant TRPV4 mice exhibit focal BSCB dysfunction, associated with a gain-of-function in TRPV4 channel activity in NVECs, that drives the subsequent degeneration of motor neurons.

RESULTS:

Mutant TRPV4 mice develop marked neurological phenotypes

We generated two mouse models of TRPV4 channelopathy by introducing the R269C or R232C mutations into the endogenous mouse *Trpv4* gene (fig. S1). These two mutations were selected as both cause dSMA and CMT2 (5, 10–12, 19, 20), and are located at an exposed arginine residue on the convex face of the TRPV4 ankyrin repeat domain, a feature shared by the majority of neurological disease-causing mutations (14, 15) (fig. S1A). Our characterization of these two lines revealed comparable phenotypes (outlined below) in homozygous *Trpv4*^{R269C} (*Trpv4*$^{R269C/R269C}$) and heterozygous *Trpv4*^{R232C} (*Trpv4*$^{R232C/+}$) knock-in mice, consistent with the stronger effect of the R232C mutation on channel activity observed in heterologous expression studies (fig. S1, B and C). The *Trpv4*^{R269C} line was generated using a targeting vector in which *Trpv4* exons 4 and 5 were flanked by loxP sites to enable Cre recombinase (Cre)-mediated gene deletion (fig. S1D), whereas the *Trpv4*^{R232C} mutation was introduced utilizing CRISPR/Cas9 gene editing (fig. S1E). As in heterologous expression systems (5), introduction of disease-causing mutations did not alter TRPV4 transcript (fig. S1, F and G) and protein expression in vivo (fig. S1, H and I).

Trpv4$^{R269C/R269C}$ mice were born at the expected Mendelian ratio (table S1) but exhibited motor behavioral deficits with onset in the third postnatal week (Fig. 1, A and B, fig. S2, A to C) and lethality by weaning age (Fig. 1C). Motor deficits manifested initially as mild impairments in behavioral assays (defined here as *Stage A*; fig. S2A) but progressed during the 24–36 hours preceding death to include forelimb-predominant paralysis (often asymmetric), kyphosis, and difficulty maintaining upright head posture (defined here as *Stage B*; Fig. 1A, fig. S2A, movie S1). In the hours preceding death, mutant animals lost the ability to ambulate and then exhibited labored breathing (defined here as *Stages C* and *D*, respectively; fig. S2A). Comparable motor behavioral and lethality phenotypes were observed in *Trpv4*$^{R232C/+}$ mice (fig. S2, D and E, movie S2).

Spinal motor neuron degeneration in TRPV4 mutant mice

Given the pronounced neck and forelimb motor behavioral deficits, we performed histopathological assessments of the cervical spinal cord and associated musculature. Examination of cervical spinal cord level 1 (C1) in symptomatic *Trpv4*$^{R269C/R269C}$ mutant mice at *Stage C* revealed focal motor neuron loss (Fig. 1, D to F, fig. S3, A and B; fig. S4) and proximal axon pathology (for example, swellings and fragmentation, Fig. 1G, fig. S3, C and D). Assessment of additional cervical (C2, C3, C8) and lumbar (L4, L5) spinal cord levels of *Stage C* mice revealed evidence of proximal axon pathology in C2 and C3, with no evidence of motor neuron loss at these levels (fig. S4). Consistent with these findings, neuromuscular junction (NMJ) denervation was observed in neck muscles innervated by motor neurons of the upper cervical spinal cord (Fig. 1, H and I, fig. S5, A and C), but was absent from forelimb muscles innervated by motor neurons of the lower cervical spinal cord (fig. S5, B and D). Assessment of symptomatic *Trpv4*$^{R269C/R269C}$ mice at *Stage B* revealed limited pathology in the upper cervical spinal cord (Fig. 1, J to L). Electrophysiological examination of *Stage B* mice utilizing an ex vivo spinal cord preparation, however, revealed markedly diminished monosynaptic sensory-motor reflexes at upper cervical spinal cord levels (Fig. 1M; fig. S6, A to C). Together, these data indicate that motor behavioral deficits in mutant mice are associated with motor neuron dysfunction and subsequent neurodegeneration.

Genetic deletion of the mutant allele from endothelial cells rescues TRPV4 mutant mice

To interrogate the cellular basis of the neurological phenotypes exhibited by *Trpv4*$^{R269C/R269C}$ mice, we adopted an unbiased approach of crossing the line to a series of 13 well-validated Cre mouse strains (table S2) to selectively delete the mutant allele in a cell type-specific manner. These Cre strains were selected to cover the key cell types comprising the neuromuscular unit (neurons, glia, muscle, and endothelial cells). Strikingly, marked rescue of mutant mice from lethality was only observed following endothelial cell-specific deletion of the mutant allele by crossing to two independent Cre-expressing mouse strains (*Cdh5*^{Cre}, *Tie2*^{Cre}; Fig. 2, A and B, fig. S7, A to K, S8, A to D). As *Cdh5*^{Cre} and *Tie2*^{Cre} alleles also show expression in a subset of microglia (21), we examined the effects of deletion of the mutant allele from microglia (and other myeloid cells) by crossing to the *Lyz2*^{Cre} mouse strain, and observed no effect on survival (fig. S7H). In addition to improved survival, endothelial cell-specific *Trpv4*^{R269C} deletion abrogated motor behavioral deficits in both weanling (Fig. 2C; fig. S8A, S8, C and D) and adult mice (Fig. 2D; fig. S8B, movie S3), as well as C1 motor neuron loss (Fig. 2E, fig. S8E) and proximal axon pathology (fig. S8F). Biochemical examination confirmed knockdown of *Trpv4* expression in CNS vessels isolated from *Trpv4*$^{R269C/R269C}$ mice expressing *Cdh5*^{Cre} or *Tie2*^{Cre} (Fig. 2, F and G). To confirm *Trpv4* expression in NVECs, we utilized a *Trpv4* reporter mouse line in which Cre-ERT2 is generated under the control of the endogenous *Trpv4* promoter and can initiate, following tamoxifen administration, production of tdTomato from a ROSA26-STOP$^{fl/fl}$-tdTomato allele (fig. S9, A and B). Expression of the tdTomato reporter was observed in NVECs (CD31^{+}, Tie2-GFP^{+}) of the spinal cord and brain (Fig. 2, H to J; fig. S9, C to I), consistent with recent single-cell RNA-sequencing (scRNA-seq) (22–27) and electrophysiology (28) studies. Assessment of tdTomato expression in C1 spinal cord revealed expression principally in NVECs (Fig. 2J) of small caliber vessels (fig. S9C), with

enrichment in the grey matter and the ventral horn (fig. S9, D and E), the territory of the sulcal artery (29). NVECs expressing the tdTomato reporter were also observed to occur in higher numbers in C1 spinal cord than in lumbar (L4–5) regions (fig. S9F).

Mutant TRPV4 channels are overactive in NVECs

To characterize mutant TRPV4 channel activity in NVECs, we performed ratiometric calcium imaging of primary NVECs isolated from the brain and spinal cord of *Trpv4*$^{R269C/R269C}$ mice and WT littermates (Fig. 3, A to E). Application of the TRPV4-specific agonist GSK1016790A (GSK101) resulted in elevations in cytosolic free calcium in NVECs from *Trpv4*$^{R269C/R269C}$ mice that were of greater amplitude and shorter latency than those observed in NVECs from WT littermates (Fig. 3, C to E). Differences in basal cytosolic free calcium were not observed (fig. S10A). Comparable results were obtained from NVECs cultured from *Trpv4*$^{R232C/+}$ mice (fig. S10, B to E). Whole-cell patch clamp electrophysiology further revealed increased current density in *Trpv4*$^{R269C/R269C}$ NVECs compared to WT cells following GSK101 application (Fig. 3, F and G), with subsequent perfusion of the TRPV4-specific antagonist GSK2193874 (GSK219) (30) confirming the specificity of the responses to GSK101 (Fig. 3, F and G). To assess the effects of mutant TRPV4 channel activity on NVEC barrier function, we assessed transendothelial electrical resistance (TEER; a measure of barrier integrity) in confluent monolayers of cultured NVECs. NVEC monolayers from *Trpv4*$^{R269C/R269C}$ and WT mice exhibited equivalent TEER values at baseline (*Trpv4*^{WT}, 59 ± 14.55 Ω cm^2; *Trpv4*$^{R269C/R269C}$, 62.33 ± 11.94 Ω cm^2; mean ± SEM, unpaired two-sided *t*-test, p=0.86; n=6 isolations/genotype), but decreases in TEER following application of GSK101 (Fig. 3H). Comparison of WT and mutant monolayers revealed that the mutant channel mediated a more rapid decline in TEER at lower doses of GSK101 (50 nM, Fig. 3H), with no difference between genotypes observed at higher doses (500 nM, Fig. 3H). Importantly, WT and mutant monolayers both exhibited an equivalent recovery of barrier function when measured at 24 hrs post-GSK101 application (Fig. 3I). Together, these data demonstrate that TRPV4 mutant channels exhibit a gain-of-function in channel activity in NVECs, resulting in a more rapid decline in barrier integrity following channel activation.

Mutant TRPV4 expression in endothelial cells causes focal BSCB breakdown

We next investigated whether symptomatic *Trpv4*$^{R269C/R269C}$ mice exhibit impairments of NVEC barrier function in vivo, and whether these may be linked to the motor behavioral and histopathological phenotypes of mutant mice. Blood-CNS barrier integrity was assessed utilizing three complementary approaches: i. intraperitoneal injection of EZ-Link Sulfo-NHS-LC-Biotin (EZ-Biotin), a low molecular weight tracer (mw, 0.56 kDa) that does not cross intact blood-CNS barriers (31), ii. immunohistochemical detection of the leak of endogenous fibrinogen (mw, 340 kDa) into the CNS parenchyma from the systemic circulation, and iii. immunohistochemical detection of extravascular leak of endogenous IgG (mw, 150 kDa). Symptomatic *Trpv4*$^{R269C/R269C}$ mice at *Stage B* exhibited marked, often asymmetric, leakage of all three molecules, most prominently within the upper cervical spinal cord (Fig. 4, A to E, fig. S11, S12) and brainstem (fig. S11B, S12). BSCB leakage was reduced or absent at lower cervical and lumbar spinal cord levels (fig. S12) and absent from cortex, hippocampus, and cerebellum (fig. S11B, S13, A to F). The regional

distribution of leak across the CNS was confirmed in whole mount preparations from symptomatic mutant mice injected with the tracer Evans blue (fig. S11A). Endothelial barrier leak was not detected in mutant mice in the retina (*Stage B-C*; fig. S14, A to D) or distal colon (*Stage B-C*; fig. S14, E to H), where TRPV4 has previously been demonstrated to regulate barrier function (32, 33).

Importantly, impairments of BSCB integrity were not observed in presymptomatic mice and were absent from mutant mice expressing *Cdh5*^{Cre} or *Tie2*^{Cre} (Fig. 4, A to E, G and H, fig. S12), linking barrier breakdown to the motor behavioral and lethality phenotypes. BSCB leak in the upper cervical spinal cord was most extensive within the ventral horn (Fig. 4F; fig. S11C) adjacent to motor neuron somata (Fig. 4B; fig. S11D), a pattern also observed in symptomatic *Trpv4*$^{R232C/+}$ mice (fig. S11E). Assessments of the vasculature of the C1 spinal cord ventral horn in presymptomatic *Trpv4*$^{R269C/R269C}$ (postnatal day 15) mice did not reveal abnormalities of vascular patterning (Fig. 4I, fig. S15, A to D) or pericyte coverage (fig. S15, E to G). Consistent with mutant TRPV4 channels impairing BSCB function, blood vessels at sites of EZ-Biotin extravasation in C1 spinal cord of symptomatic *Trpv4*$^{R269C/R269C}$ mice (*Stage B*) exhibited focal loss of the tight junction protein zonula occludens-1 (ZO-1, Fig. 5, A and B). In contrast, neighboring C1 spinal cord blood vessels not demonstrating BSCB breakdown exhibited equivalent ZO-1 expression to the C1 vasculature of *Trpv4*^{WT} mice (Fig. 5, A and B). Ultrastructural examination of symptomatic *Trpv4*$^{R269C/R269C}$ mice (*Stages B-C*) also revealed discontinuities of NVEC tight junction complexes in the upper cervical spinal cord ventral horn (Fig. 5, C and D), comparable to those described previously in cortical NVECs in a mouse model of stroke (34).

TRPV4 antagonist administration rescues symptomatic mutant mice

To determine whether the neurological phenotypes of *Trpv4*$^{R269C/R269C}$ mice were reversible upon TRPV4 inhibition, we assessed the effects of systemic administration of the TRPV4-specific antagonist GSK219. Previous work has shown that chronic dosing of rodents with GSK219 at concentrations sufficient to maintain maximal TRPV4 inhibition has no effect on mean arterial pressure, heart rate, plasma electrolytes, or creatine clearance (30). We elected to initiate treatment once the mutant mice reached symptomatic phase *Stage B* (P17–21, age range at treatment onset; P18.7 ± 0.4, *Trpv4*$^{R269C/R269C}$ + vehicle, P18.8 ± 0.2, *Trpv4*$^{R269C/R269C}$ + 0.5 mg/kg GSK219, P19.9 ± 0.3, *Trpv4*$^{R269C/R269C}$ + 2 mg/kg GSK219, mean ± SEM), a stage characterized by leakage of serum products, motor behavioral deficits and motor neuronal dysfunction, but limited motor neuron soma loss (Fig. 1; fig. S3). Symptomatic *Trpv4*$^{R269C/R269C}$ mice (*Stage B*) treated systemically with GSK219 (0.5–2 mg/kg; twice daily intraperitoneal injections) exhibited marked improvements in both survival (Fig. 6A) and motor behavior (Fig. 6, B and C; movie S4), with mice receiving the highest dose (2 mg/kg) showing near complete rescue. To interrogate whether GSK219 administration had reversed BSCB breakdown, we assessed GSK219-treated mutant mice at P50–60 (37.6 ± 1.2 days of treatment, mean ± SEM) for evidence of EZ-Biotin tracer leak within the nervous system. As in Cre-rescued mutant mice, EZ-Biotin extravasation was not detected in the upper cervical spinal cord of GSK219-treated mice (Fig. 6, D and E), demonstrating rescue of BSCB function. Assessments

of ZO-1 immunoreactivity in the vasculature of the C1 spinal cord of *Trpv4*$^{R269C/R269C}$ mice treated for 10 days with GSK219 (2 mg/kg; twice daily intraperitoneal injections) also revealed restoration of the expression of this key tight junction protein (Fig. 6F). No improvements in survival, motor behavior, or BSCB function were detected in vehicle-treated mutant mice (Fig. 6, A to E). Histopathological assessments of GSK219-treated mice at P50–60 revealed no motor neuron loss nor proximal axon pathology in C1 spinal cord (Fig. 6, G to I). Together, these data demonstrate that GSK219 treatment restored BSCB integrity in symptomatic mutant mice, rescued survival and motor behavioral phenotypes, and afforded strong protection against motor neuron loss and axonal pathology.

DISCUSSION

Here, we report an unanticipated role for mutant TRPV4 ion channels in NVECs that impacts spinal motor neuron integrity in a non-cell autonomous manner through focal disruption of the BSCB. These findings underscore the key role that NVECs can assume in neurological disorders, including neurodegenerative disease, and identify TRPV4 as an important regulator of BSCB permeability. *Trpv4*$^{R269C/R269C}$ mice exhibited an age-dependent barrier breach permitting the flux of blood constituents of a broad range of sizes (at least 0.56–340 kDa) into select CNS regions, resulting in successive stages of neuronal dysfunction and loss. Extravasated proteins included fibrinogen, a coagulation factor that can initiate neurodegenerative processes (for example, dendritic spine loss) upon entry into the CNS parenchyma (35, 36). The spontaneous, postnatal nature of the barrier deficits is supported by the absence of barrier hyperpermeability prior to symptom onset, and by the reversal of phenotypes following antagonist administration. To our knowledge, the current findings represent the first example of a human genetic mutation causing acquired blood-CNS barrier breakdown as the primary driver of neurodegenerative pathology. In contrast, other monogenic neurological diseases caused by mutations of key endothelial cell proteins (for example, occludin, JAM3, ESAM, CCM1–3, SLC2A1) involve marked structural abnormalities, angiopathy, or severe hemorrhaging (37–40). These differences may reflect the role of TRPV4 as a modulator of barrier integrity, rather than as an integral component of NVEC intercellular junctional complexes.

Consistent with recent scRNA-seq studies (22–27), our examination of a *Trpv4* reporter mouse line revealed *Trpv4* expression in NVECs but absence of expression in spinal motor neurons. Recently published work examining an independent *Trpv4* reporter mouse line has described comparable findings (41). Importantly, several scRNA-seq studies of human brain and spinal cord have also revealed *TRPV4* expression in NVECs (42–46), but not motor neurons (47), highlighting the relevance of the findings described here to patients with dSMA/CMT2. Also consistent across studies of both mouse and human CNS tissues is that TRPV4 appears to be expressed in only a subset of NVECs. Of note, a recent scRNA-seq study of the coronary artery identified a distinct TRPV4-expressing endothelial cell subpopulation (48). Functionally, endothelial cells of this TRPV4^{+} subpopulation differ from other coronary artery endothelial cell types in exhibiting calcium responses to fluid shear stress (48). As calcium flux through TRPV4 in endothelial cells can lead to the generation of intercellular calcium waves through purinergic signalling (49), TRPV4 activation in a small number of endothelial cells may have broader functional impacts. The specific properties of

TRPV4-expressing NVECs, and how they may influence neighboring NVECs, remain to be determined.

Our immunohistochemical assessments of ZO-1 revealed focal loss of this key NVEC tight junction protein at sites of BSCB breakdown in symptomatic *Trpv4*$^{R269C/R269C}$ mice, consistent with the discontinuities of NVEC tight junction complexes detected at the ultrastructural level. Together, these data suggest that local reductions in tight junction integrity may contribute to BSCB hyperpermeability in symptomatic TRPV4 mutant mice. Reduced expression and mislocalization of NVEC tight junction proteins, as well as ultrastructural abnormalities of NVEC tight junction complexes, have been described in other neurodegenerative disorders associated with blood-CNS barrier impairments, including stroke, Alzheimer's disease, and Huntington's disease (50). The restoration of ZO-1 expression and abrogation of BSCB hyperpermeability following treatment with the TRPV4-specific antagonist GSK219 suggest that BSCB breakdown is driven principally by mutant TRPV4 channel activity in *Trpv4*$^{R269C/R269C}$ mice. Consistent with this concept, NVECs isolated and cultured from the upper cervical spinal cord and brainstem of both *Trpv4*$^{R269C/R269C}$ and *Trpv4*$^{R232C/+}$ mice exhibited elevated TRPV4 channel activity. Elucidation of the molecular pathways by which mutant TRPV4 channel activity alters NVEC tight junction integrity and barrier function will be an important focus for future work. We and others have shown that TRPV4 interacts with the small GTPase RhoA (14, 16, 17) and that motor neuron disease-causing mutations in TRPV4 disrupt this binding and the reciprocal inhibitory interactions between TRPV4 and RhoA (14, 16). As RhoA activation can drive endothelial junctional complex disassembly by promoting actin cytoskeleton remodeling (51, 52), these findings suggest a potential mechanism through which TRPV4 may regulate BSCB permeability. Inhibition of TRPV4 in endothelial cells by GSK219 may normalize RhoA activation and thereby enable junctional complex reassembly through endogenous repair pathways (53).

One feature of the BSCB impairments exhibited by TRPV4 mutant mice is their regional specificity, with leak occurring most prominently in the ventral horn of the upper cervical spinal cord. Recent work has revealed considerable heterogeneity in both the transcriptomes and barrier properties of endothelial cell populations within different brain regions (44, 54–56). Little is known, however, about how NVECs of the spinal cord may differ from those of the brain or between different spinal cord regions. TRPV4 responses are tightly regulated by channel density, plasma membrane composition, and the stoichiometry of the channel in relation to its binding partners, each of which may vary between NVECs of different CNS regions. Indeed, our assessment of *Trpv4* reporter mice revealed higher numbers of NVECs expressing the tdTomato reporter in upper cervical (C1) compared to lumbar (L4–5) spinal cord, suggesting that differences in expression may represent one factor contributing to the observed regionality. As TRPV4 is activated, either directly or indirectly, by a number of environmental (for example, fluid shear stress) and chemical (for example, arachidonic acid metabolites) stimuli, local differences in the nature of these stimuli may also contribute to the regional specificity. Previous histological studies have identified the ventral horn, within the territory of the sulcal artery, as a primary site of serum protein leak in mouse models of the motor neuron disease amyotrophic lateral sclerosis (ALS) (57, 58), suggesting that the BSCB in this region may be particularly susceptible to disruption. As the dorsal

and ventral portions of the spinal cord are perfused by separate arterial systems (29), an important subject for future study will be an investigation of the barrier properties of these two vascular beds.

Although breakdown of blood-neural barriers of the central and peripheral nervous systems has been implicated in the pathogenesis of numerous neurodegenerative diseases (1–4), elucidation of the exact contributions of barrier disruption to neuronal dysfunction and degeneration has proven difficult due to the complex aetiologies of these disorders. Blood-neural barrier disruption has been implicated, for example, in the pathogenesis of both acute and chronic forms of peripheral neuropathy, including diabetic neuropathy, inflammatory neuropathy, traumatic nerve injury, and neuropathic pain (4, 59–68). As detailed above, BSCB breakdown has also been implicated in the pathogenesis of ALS (57, 69–71), with work in the $SOD1^{G93A}$ mouse model demonstrating that treatments promoting BSCB integrity can delay the onset of motor behavioral impairments and rescue early changes in spinal motor neuron neurite density (57, 70). A growing body of work in Alzheimer's disease has also identified NVEC alterations, such as downregulation of LRP1 expression (72), that drive blood-CNS barrier impairments and contribute to neurodegenerative phenotypes (36, 73–76). The findings of the present study advance our understanding of the role of blood-CNS barrier impairments in neurodegenerative disease by providing the first example of motor neuron degeneration triggered by spontaneous BSCB breakdown.

Patients with TRPV4-mediated motor neuron disease exhibit heterogeneity in age of onset, disease severity, and clinical manifestations; with no clear genotype-phenotype correlation (5, 9–12). In generating mouse models of these disorders, we selected two mutations ($Trpv4^{R269C}$, $Trpv4^{R232C}$) that can each cause both dSMA and CMT2 (5, 10–12, 19, 20). The two mouse lines exhibited very similar motor behavioral, BSCB hyperpermeability, and lethality phenotypes. As mutant mice exhibit either full ($Trpv4^{R269C}$) or near-full lethality ($Trpv4^{R232C}$) by weaning age, these lines mirror the severe end of the clinical spectrum of TRPV4-mediated motor neuron disease. As TRPV4-mediated motor neuron disease is a relatively rare disorder, little CNS tissue from patients is currently available. Future studies will be required to characterize BSCB impairments in humans. Nonetheless, this study highlights the therapeutic potential of small molecule TRPV4 antagonism for treatment of patients harboring TRPV4 mutations. Treatment of $Trpv4^{R269C}$ mice at a symptomatic disease stage afforded a dose-dependent rescue from lethality. Our combined genetic and pharmacological data are consistent with TRPV4 blockade enabling NVECs to fully re-establish barrier integrity thus allowing reparative processes within the CNS parenchyma. Similarly, TRPV4 antagonists have previously been shown to improve outcomes in rodent models of injury and disease associated with endothelial hyperpermeability in several tissue types (30, 33, 77–79).

An orally bioavailable TRPV4 antagonist has been well-tolerated in phase I and II clinical trials (NCT02119260, NCT02497937, NCT03372603, and NCT04292912) (80–82). Of particular relevance to the present study, the intended site of pharmacological action in three of these clinical trials (NCT02119260, NCT02497937, and NCT04292912) was vascular endothelial cells (81, 82). Using an ex vivo impedance assay to assess target engagement, oral dosing of a TRPV4 antagonist in both human patients with heart failure and healthy

subjects was found to provide circulating drug concentrations sufficient to inhibit TRPV4 activation in cultured endothelial cells (83). These findings suggest that TRPV4 inhibition within endothelial cells can be achieved in human patients without accompanying side effects or adverse events. In further support of the translational feasibility of TRPV4 inhibition in human patients, TRPV4-null mice exhibit only subtle phenotypes (13, 84), such as reduced sensitivity to sour taste (85), increased bladder capacity (86, 87), and increased bone mass (88), but do not exhibit evidence of motor behavioral deficits (89) or neuropathology (90).

Our study has limitations that should be considered. The Cre mouse strains utilized to delete the *Trpv4*^{R269C} allele from endothelial cells express Cre in a pan-endothelial manner and thus do not enable discrimination between potential contributions of neuronal and non-neuronal endothelial cells to observed phenotypes. Although the regionality and asymmetry of BSCB breakdown in symptomatic mutant mice strongly suggest that the neurological phenotypes arise due to direct effects of mutant TRPV4 in NVECs it will be important to verify this experimentally. We cannot completely exclude that abnormalities of other organ systems contribute to lethality in mutant mice, though necropsy examinations have not revealed consistent pathological abnormalities anticipated to cause early lethality (Table S3). Though this study identifies TRPV4 as a key regulator of BSCB integrity, further work will also be required to identify molecular pathways mediating the effects of TRPV4 on BSCB structure and function. A detailed understanding of these mechanisms will also provide insights into whether these pathways may be shared across multiple forms of neurodegenerative disease, as well as into potential roles of TRPV4 in regulating BSCB integrity in other neurological disorders. Further studies will also be necessary to determine the capacity of TRPV4 small molecule antagonists to ameliorate clinical symptoms in patients with dSMA/CMT2 and how early in disease they may need to be delivered to exhibit efficacy.

In summary, though it has been recognized that motor neuron disease-causing mutations alter TRPV4 channel activity it has remained unclear how expression of mutant TRPV4 channels in vivo precipitates neurodegeneration. We demonstrate that neuropathology in mouse models of TRPV4 channelopathy is driven in a non-cell autonomous manner by effects of mutant TRPV4 channels in endothelial cells. TRPV4 mutant mice exhibit focal BSCB breakdown associated with motor behavioral impairments, regional motor neuron loss, and early lethality. Treatment of symptomatic TRPV4 mutant mice with a TRPV4-specific antagonist provided a rescue of each of these phenotypes. Together, these findings highlight TRPV4 small molecule antagonism as a potential disease-modifying therapeutic for patients with TRPV4-mediated motor neuron disease, and potentially other neurological diseases characterized by impairments of BSCB integrity.

MATERIALS AND METHODS:

Study design

The objective of this study was to investigate the cellular basis of TRPV4-mediated neurological phenotypes in vivo, and to assess their potential reversibility. We generated and characterized two mouse models in which different disease-causing mutations

(R269C, R232C) were introduced into the endogenous mouse *Trpv4* gene. TRPV4 mutant mice were assessed using motor behavioral assays, histopathology, spinal cord electrophysiology, genetic deletion studies, BCNSB tracer studies, and transmission electron microscopy. NVECs isolated and cultured from mutant mice were examined by ratiometric calcium imaging, TEER, and whole-cell patch clamp electrophysiology. The reversibility of neurological phenotypes in TRPV4 mutant mice was assessed by examining the effects of systemic administration of the TRPV4-specific antagonist GSK219. Please see Supplementary Materials and Methods for further details. All experimental procedures were approved by the Institutional Animal Care and Use Committees of Johns Hopkins University and the University of Rhode Island and were performed in compliance with National Institute of Health guidelines for the care and use of laboratory animals. Mouse expressing the $Trpv4^{R269C}$ and $Trpv4^{R232C}$ alleles were generated at The Jackson Laboratory using procedures approved by the Institutional Animal Care and Use Committee. All animals were housed at 22°C and 42% humidity in a 14/10-h light–dark cycle with *ad libitum* access to food and water. Quantification of motor neuron numbers, NMJ denervation, and blood-CNS barrier leak was performed by experimenters blinded to genotype and treatment. All imaging for quantification of fluorescence intensity was performed using the same microscope, exposure times and laser/lamp intensities across the entire set of sections per experiment. Sample sizes were selected based on pilot studies within our laboratories, and our prior studies of other mouse models of spinal muscular atrophy (91). No randomization was employed. Experimenters were not blinded to genotype for motor behavioral assessments. Male and female mice, littermates wherever possible, were utilized for all experiments.

Statistical analysis

Statistical tests, significance levels, and sample sizes are detailed in each figure legend. Statistical analyses were performed using GraphPad Prism 9.0 software. Data are presented as means ± SEM, with individual data points also plotted in column graphs. Statistical comparisons between two groups were performed by unpaired two-sided *t*-test (for equal variances) or by unpaired two-sided *t*-test with Welch's correction (for unequal variances). Differences among three or more groups were assessed by one-way analysis of variance (ANOVA) followed by Tukey's or Dunnett's multiple comparison test. Two-way ANOVA was used for statistical analysis of spinal cord electrophysiology, longitudinal TEER, longitudinal motor behavioral, RT-qPCR, and blood-brain barrier leakage studies. Chi-square analysis was used to assess Mendelian ratios. P values ≤ 0.05 were considered statistically significant.

Supplementary Material

Refer to Web version on PubMed Central for supplementary material.

Acknowledgments:

We thank Mark Rich for preliminary assessments of the neuromuscular junctions of TRPV4 mutant mice, Klaus-Armin Navé for kindly providing $Cnp^{tm1(cre)Kan}$ mice, the Phenotyping and Pathology Core of Johns Hopkins University School of Medicine for performing necropsy examinations, and Jeremy Nathans for reading and providing comments on the manuscript.

Funding:

This work was supported by: Muscular Dystrophy Association grant 629305 to C.J.S.; Muscular Dystrophy Association grant 2777551 to C.J.S.; National Institutes of Health grant R35NS122306 to C.J.S.; National Institutes of Health grant R211NS087579 to C.J.S.; National Institutes of Health grant R35GM124824 to Z.Q.; National Institutes of Health grant R01NS118014 to Z.Q.; National Institutes of Health grant RF1NS134549 to Z.Q.; National Institutes of Health grant R01NS106008 to P.C.S.; National Institutes of Health grant R61/33 HL154252 to P.C.S.; National Institute of Neurological Disorders and Stroke grant R01NS104436 to K.A.Q.; National Institute of Neurological Disorders and Stroke grant R01NS132728 to K.A.Q.; a New Discovery Award from Advance-CTR, supported by IDeA-CTR grant U54GM115677, to K.A.Q.; and a Pamela Mars Wright Innovator Award to J.M.S.

REFERENCES AND NOTES:

1. Sweeney MD, Kisler K, Montagne A, Toga AW, Zlokovic BV, The role of brain vasculature in neurodegenerative disorders. Nat. Neurosci. 21, 1318–1331 (2018). [PubMed: 30250261]
2. Liebner S. et al. , Functional morphology of the blood-brain barrier in health and disease. Acta Neuropathol. 135, 311–336 (2018). [PubMed: 29411111]
3. Profaci CP, Munji RN, Pulido RS, Daneman R, The blood-brain barrier in health and disease: Important unanswered questions. J. Exp. Med. 217, e20190062 (2020).
4. Echeverry S, Shi XQ, Rivest S, Zhang J, Peripheral nerve injury alters blood-spinal cord barrier functional and molecular integrity through a selective inflammatory pathway. J. Neurosci. 31, 10819–10828 (2011). [PubMed: 21795534]
5. Landouré G. et al. , Mutations in TRPV4 cause Charcot-Marie-Tooth disease type 2C. Nat. Genet. 42, 170–174 (2010). [PubMed: 20037586]
6. Deng HX et al. , Scapuloperoneal spinal muscular atrophy and CMT2C are allelic disorders caused by alterations in TRPV4. Nat. Genet. 42, 165–169 (2010). [PubMed: 20037587]
7. Auer-Grumbach M. et al. , Alterations in the ankyrin domain of TRPV4 cause congenital distal SMA, scapuloperoneal SMA and HMSN2C. Nat. Genet. 42, 160–164 (2010). [PubMed: 20037588]
8. Chen DH et al. , CMT2C with vocal cord paresis associated with short stature and mutations in the TRPV4 gene. Neurology 75, 1968–1975 (2010). [PubMed: 21115951]
9. McEntagart M, TRPV4 axonal neuropathy spectrum disorder. J. Clin. Neurosci. 19, 927–933 (2012). [PubMed: 22617546]
10. Zimon M. et al. , Dominant mutations in the cation channel gene transient receptor potential vanilloid 4 cause an unusual spectrum of neuropathies. Brain. 133, 1798–1809 (2010). [PubMed: 20460441]
11. Echaniz-Laguna A. et al. , Phenotypic spectrum and incidence of TRPV4 mutations in patients with inherited axonal neuropathy. Neurology 82, 1919–1926 (2014). [PubMed: 24789864]
12. Berciano J. et al. , Reduced penetrance in hereditary motor neuropathy caused by TRPV4 Arg269Cys mutation. J. Neurol. 258, 1413–1421 (2011). [PubMed: 21336783]
13. White JP et al. , TRPV4: Molecular Conductor of a Diverse Orchestra. Physiol. Rev. 96, 911–973 (2016). [PubMed: 27252279]
14. Kwon DH et al. , TRPV4-Rho GTPase complex structures reveal mechanisms of gating and disease. Nat Commun 14, 3732 (2023). [PubMed: 37353484]
15. Sullivan JM et al. , Novel mutations highlight the key role of the ankyrin repeat domain in TRPV4-mediated neuropathy. Neurol. Genet. 1, e29 (2015). [PubMed: 27066566]
16. McCray BA et al. , Neuropathy-causing TRPV4 mutations disrupt TRPV4-RhoA interactions and impair neurite extension. Nat. Commun. 12, 1444 (2021). [PubMed: 33664271]
17. Nadezhdin KD et al. , Structure of human TRPV4 in complex with GTPase RhoA. Nat. Commun. 14, 3733 (2023). [PubMed: 37353478]
18. Fecto F. et al. , Mutant TRPV4-mediated toxicity is linked to increased constitutive function in axonal neuropathies. J. Biol. Chem. 286, 17281–17291 (2011). [PubMed: 21454511]
19. Klein CJ et al. , TRPV4 mutations and cytotoxic hypercalcemia in axonal Charcot-Marie-Tooth neuropathies. Neurology 76, 887–894 (2011). [PubMed: 21288981]
20. Fiorillo C. et al. , TRPV4 mutations in children with congenital distal spinal muscular atrophy. Neurogenetics 13, 195–203 (2012). [PubMed: 22526352]

21. Huang W. et al. , Critical endothelial regulation by LRP5 during retinal vascular development. PLoS One 11, e0152833 (2016).
22. Vanlandewijck M. et al. , A molecular atlas of cell types and zonation in the brain vasculature. Nature 554, 475–480 (2018). [PubMed: 29443965]
23. Consortium TTM, Single-cell transcriptomics of 20 mouse organs creates a Tabula Muris. Nature 562, 367–372 (2018). [PubMed: 30283141]
24. Sabbagh MF et al. , Transcriptional and epigenomic landscapes of CNS and non-CNS vascular endothelial cells. eLife 7, e36187 (2018).
25. Munji RN et al. , Profiling the mouse brain endothelial transcriptome in health and disease models reveals a core blood-brain barrier dysfunction module. Nat. Neurosci. 22, 1892–1902 (2019). [PubMed: 31611708]
26. Kalucka J. et al. , Single-Cell transcriptome atlas of murine endothelial cells. Cell 180, 764–779 e720 (2020). [PubMed: 32059779]
27. Yu M. et al. , Integrative multi-omic profiling of adult mouse brain endothelial cells and potential implications in Alzheimer's disease. Cell Rep. 42, 113392 (2023).
28. Harraz OF, Longden TA, Hill-Eubanks D, Nelson MT, PIP2 depletion promotes TRPV4 channel activity in mouse brain capillary endothelial cells. eLife 7, e38689 (2018).
29. Thron AK, Vascular anatomy of the spinal cord (Springer-Verlag, Wien; New York, 2016), pp. 114 p.
30. Thorneloe KS et al. , An orally active TRPV4 channel blocker prevents and resolves pulmonary edema induced by heart failure. Sci. Transl. Med. 4, 159ra148 (2012).
31. Wang Y. et al. , Norrin/Frizzled4 signaling in retinal vascular development and blood brain barrier plasticity. Cell 151, 1332–1344 (2012). [PubMed: 23217714]
32. Phuong TTT et al. , Calcium influx through TRPV4 channels modulates the adherens contacts between retinal microvascular endothelial cells. J. Physiol. 595, 6869–6885 (2017). [PubMed: 28949006]
33. Matsumoto K. et al. , Transient receptor potential vanilloid 4 channel regulates vascular endothelial permeability during colonic inflammation in dextran sulphate sodium-induced murine colitis. Br. J. Pharmacol. 175, 84–99 (2018). [PubMed: 29053877]
34. Knowland D. et al. , Stepwise recruitment of transcellular and paracellular pathways underlies blood-brain barrier breakdown in stroke. Neuron 82, 603–617 (2014). [PubMed: 24746419]
35. Merlini M. et al. , Fibrinogen induces microglia-mediated spine elimination and cognitive impairment in an Alzheimer's disease model. Neuron 101, 1099–1108 (2019). [PubMed: 30737131]
36. Ryu JK et al. , Fibrin-targeting immunotherapy protects against neuroinflammation and neurodegeneration. Nat. Immunol. 19, 1212–1223 (2018). [PubMed: 30323343]
37. Sweeney MD, Zhao Z, Montagne A, Nelson AR, Zlokovic BV, Blood-brain barrier: From physiology to disease and back. Physiol. Rev. 99, 21–78 (2019). [PubMed: 30280653]
38. Lecca M. et al. , Bi-allelic variants in the ESAM tight-junction gene cause a neurodevelopmental disorder associated with fetal intracranial hemorrhage. Am. J. Hum. Genet. 110, 681–690 (2023). [PubMed: 36996813]
39. Tang M. et al. , An early endothelial cell-specific requirement for Glut1 is revealed in Glut1 deficiency syndrome model mice. JCI Insight 6, e145789 (2021).
40. Winkler EA et al. , GLUT1 reductions exacerbate Alzheimer's disease vasculo-neuronal dysfunction and degeneration. Nat. Neurosci. 18, 521–530 (2015). [PubMed: 25730668]
41. Hu X. et al. , A TRPV4-dependent neuroimmune axis in the spinal cord promotes neuropathic pain. J. Clin. Invest. 133, e161507 (2023).
42. Yadav A. et al. , A cellular taxonomy of the adult human spinal cord. Neuron 111, 328–344 e327 (2023). [PubMed: 36731429]
43. Garcia FJ et al. , Single-cell dissection of the human brain vasculature. Nature 603, 893–899 (2022). [PubMed: 35158371]
44. Yang AC et al. , A human brain vascular atlas reveals diverse mediators of Alzheimer's risk. Nature 603, 885–892 (2022). [PubMed: 35165441]

45. Winkler EA et al. , A single-cell atlas of the normal and malformed human brain vasculature. Science 375, eabi7377 (2022).
46. Sun N. et al. , Single-nucleus multiregion transcriptomic analysis of brain vasculature in Alzheimer's disease. Nat. Neurosci. 26, 970–982 (2023). [PubMed: 37264161]
47. Kumari S. et al. , Influence of membrane cholesterol in the molecular evolution and functional regulation of TRPV4. Biochem. Biophys. Res. Commun. 456, 312–319 (2015). [PubMed: 25434996]
48. Mao A. et al. , Single-cell RNA-seq reveals coronary heterogeneity and identifies $CD133^{+}TRPV4^{high}$ endothelial subpopulation in regulating flow-Induced vascular tone in mice. Arterioscler. Thromb. Vasc. Biol. 44, 653–665 (2024). [PubMed: 38269590]
49. Zhang X, Lee MD, Buckley C, Wilson C, McCarron JG, Mitochondria regulate TRPV4-mediated release of ATP. Br. J. Pharmacol. 179, 1017–1032 (2022). [PubMed: 34605007]
50. Lochhead JJ, Yang J, Ronaldson PT, Davis TP, Structure, function, and regulation of the blood-brain barrier tight junction in central nervous system disorders. Front. Physiol. 11, 914 (2020). [PubMed: 32848858]
51. Shi Y. et al. , Rapid endothelial cytoskeletal reorganization enables early blood-brain barrier disruption and long-term ischaemic reperfusion brain injury. Nat. Commun. 7, 10523 (2016). [PubMed: 26813496]
52. Radeva MY, Waschke J, Mind the gap: mechanisms regulating the endothelial barrier. Acta. Physiol. (Oxf) 222, e12860 (2018).
53. Knox EG, Aburto MR, Clarke G, Cryan JF, O'Driscoll CM, The blood-brain barrier in aging and neurodegeneration. Mol. Psychiatry 27, 2659–2673 (2022). [PubMed: 35361905]
54. Wang Y. et al. , Interplay of the Norrin and Wnt7a/Wnt7b signaling systems in blood-brain barrier and blood-retina barrier development and maintenance. Proc. Natl. Acad. Sci. U.S.A. 115, E11827–E11836 (2018). [PubMed: 30478038]
55. Cho C, Wang Y, Smallwood PM, Williams J, Nathans J, Dlg1 activates beta-catenin signaling to regulate retinal angiogenesis and the blood-retina and blood-brain barriers. eLife 8, e45542 (2019).
56. Wenzel J. et al. , Impaired endothelium-mediated cerebrovascular reactivity promotes anxiety and respiration disorders in mice. Proc. Natl. Acad. Sci. U.S.A. 117, 1753–1761 (2020). [PubMed: 31896584]
57. Zhong Z. et al. , ALS-causing SOD1 mutants generate vascular changes prior to motor neuron degeneration. Nat. Neurosci. 11, 420–422 (2008). [PubMed: 18344992]
58. Yoshikawa M, Aizawa S, Oppenheim RW, Milligan C, Neurovascular unit pathology is observed very early in disease progression in the mutant SOD1(G93A) mouse model of amyotrophic lateral sclerosis. Exp. Neurol. 353, 114084 (2022).
59. Poduslo JF, Curran GL, Dyck PJ, Increase in albumin, IgG, and IgM blood-nerve barrier indices in human diabetic neuropathy. Proc. Natl. Acad. Sci. U.S.A. 85, 4879–4883 (1988). [PubMed: 3387444]
60. Lim TKY et al. , Blood-nerve barrier dysfunction contributes to the generation of neuropathic pain and allows targeting of injured nerves for pain relief. Pain 155, 954–967 (2014). [PubMed: 24502843]
61. Ben-Kraiem A. et al. , Selective blood-nerve barrier leakiness with claudin-1 and vessel-associated macrophage loss in diabetic polyneuropathy. J. Mol. Med. (Berl) 99, 1237–1250 (2021). [PubMed: 34018017]
62. Konigs V. et al. , GPR40 activation abolishes diabetes-induced painful neuropathy by suppressing VEGF-A expression. Diabetes 71, 774–787 (2022). [PubMed: 35061031]
63. Reinhold AK et al. , MicroRNA-21–5p functions via RECK/MMP9 as a proalgesic regulator of the blood nerve barrier in nerve injury. Ann. N.Y. Acad. Sci. 1515, 184–195 (2022). [PubMed: 35716075]
64. Reinhold AK, Rittner HL, Characteristics of the nerve barrier and the blood dorsal root ganglion barrier in health and disease. Exp. Neurol. 327, 113244 (2020).
65. Liu LY et al. , Comparison of blood-nerve barrier disruption and matrix metalloprotease-9 expression in injured central and peripheral nerves in mice. Neurosci. Lett. 434, 155–159 (2008). [PubMed: 18243551]

66. Akassoglou K, Kombrinck KW, Degen JL, Strickland S, Tissue plasminogen activator-mediated fibrinolysis protects against axonal degeneration and demyelination after sciatic nerve injury. J. Cell Biol. 149, 1157–1166 (2000). [PubMed: 10831618]

67. Beggs S, Liu XJ, Kwan C, Salter MW, Peripheral nerve injury and TRPV1-expressing primary afferent C-fibers cause opening of the blood-brain barrier. Mol. Pain 6, 74 (2010). [PubMed: 21044346]

68. Montague-Cardoso K. et al. , Changes in vascular permeability in the spinal cord contribute to chemotherapy-induced neuropathic pain. Brain Behav. Immun. 83, 248–259 (2020). [PubMed: 31669344]

69. Garbuzova-Davis S. et al. , Impaired blood-brain/spinal cord barrier in ALS patients. Brain Res. 1469, 114–128 (2012). [PubMed: 22750125]

70. Winkler EA et al. , Blood-spinal cord barrier disruption contributes to early motor-neuron degeneration in ALS-model mice. Proc. Natl. Acad. Sci. U.S.A. 111, E1035–1042 (2014). [PubMed: 24591593]

71. Winkler EA et al. , Blood-spinal cord barrier breakdown and pericyte reductions in amyotrophic lateral sclerosis. Acta Neuropathol 125, 111–120 (2013). [PubMed: 22941226]

72. Nikolakopoulou AM et al. , Endothelial LRP1 protects against neurodegeneration by blocking cyclophilin A. J. Exp. Med. 218, e20202207 (2021).

73. Barisano G. et al. , Blood-brain barrier link to human cognitive impairment and Alzheimer's Disease. Nat. Cardiovasc. Res. 1, 108–115 (2022). [PubMed: 35450117]

74. Montagne A. et al. , APOE4 leads to blood-brain barrier dysfunction predicting cognitive decline. Nature 581, 71–76 (2020). [PubMed: 32376954]

75. Sweeney MD, Sagare AP, Zlokovic BV, Blood-brain barrier breakdown in Alzheimer disease and other neurodegenerative disorders. Nat. Rev. Neurol. 14, 133–150 (2018). [PubMed: 29377008]

76. Bennett RE et al. , Tau induces blood vessel abnormalities and angiogenesis-related gene expression in P301L transgenic mice and human Alzheimer's disease. Proc. Natl. Acad. Sci. U.S.A. 115, E1289–E1298 (2018). [PubMed: 29358399]

77. Zhao H. et al. , TRPV4 blockade preserves the blood-brain barrier by inhibiting stress fiber formation in a rat model of intracerebral hemorrhage. Front. Mol. Neurosci. 11, 97 (2018). [PubMed: 29636662]

78. Kumar H. et al. , Elevated TRPV4 Levels Contribute to Endothelial Damage and Scarring in Experimental Spinal Cord Injury. J. Neurosci. 40, 1943–1955 (2020). [PubMed: 31974206]

79. Michinaga S, Onishi K, Shimizu K, Mizuguchi H, Hishinuma S, Pharmacological Inhibition of Transient Receptor Potential Vanilloid 4 Reduces Vasogenic Edema after Traumatic Brain Injury in Mice. Biol. Pharm. Bull. 44, 1759–1766 (2021). [PubMed: 34719652]

80. Ludbrook VJ et al. , Adaptive study design to assess effect of TRPV4 inhibition in patients with chronic cough. ERJ Open Res. 7, 00269 (2021).

81. Goyal N. et al. , Clinical pharmacokinetics, safety, and tolerability of a novel, first-in-class TRPV4 ion channel inhibitor, GSK2798745, in healthy and heart failure subjects. Am. J. Cardiovasc. Drugs 19, 335–342 (2019). [PubMed: 30637626]

82. Stewart GM et al. , Targeting pulmonary capillary permeability to reduce lung congestion in heart failure: a randomized, controlled pilot trial. Eur. J. Heart Fail. 22, 1641–1645 (2020). [PubMed: 32227554]

83. Xu X. et al. , Identification of a human whole blood-based endothelial cell impedance assay for assessing clinical transient receptor potential vanilloid 4 target engagement ex vivo. J. Pharmacol. Exp. Ther. 376, 436–443 (2021). [PubMed: 33376150]

84. Bagnell AM, Sumner CJ, McCray BA, TRPV4: A trigger of pathological RhoA activation in neurological disease. BioEssays 44, e2100288 (2022).

85. Matsumoto K. et al. , Transient receptor potential vanilloid 4 mediates sour taste sensing via type III taste cell differentiation. Sci. Rep. 9, 6686 (2019). [PubMed: 31040368]

86. Everaerts W, Nilius B, Owsianik G, The vanilloid transient receptor potential channel TRPV4: from structure to disease. Prog. Biophys. Mol. Biol. 103, 2–17 (2010). [PubMed: 19835908]

87. Gevaert T. et al. , Deletion of the transient receptor potential cation channel TRPV4 impairs murine bladder voiding. J. Clin. Invest. 117, 3453–3462 (2007). [PubMed: 17948126]

88. Masuyama R. et al. , TRPV4-mediated calcium influx regulates terminal differentiation of osteoclasts. Cell Metab. 8, 257–265 (2008). [PubMed: 18762026]

89. Kusudo T, Wang Z, Mizuno A, Suzuki M, Yamashita H, TRPV4 deficiency increases skeletal muscle metabolic capacity and resistance against diet-induced obesity. J. Appl. Physiol. 112, 1223–1232 (2012). [PubMed: 22207724]

90. Feng X. et al. , Increased TRPV4 expression in non-myelinating Schwann cells is associated with demyelination after sciatic nerve injury. Commun. Biol. 3, 716 (2020). [PubMed: 33247229]

91. Kong L. et al. , Impaired prenatal motor axon development necessitates early therapeutic intervention in severe SMA. Sci. Transl. Med. 13, eabb6871 (2021).

92. Nilius B, Voets T, The puzzle of TRPV4 channelopathies. EMBO Rep. 14, 152–163 (2013). [PubMed: 23306656]

93. Taga A. et al. , TRPV4 mutations causing mixed neuropathy and skeletal phenotypes result in severe gain of function. Ann. Clin. Transl. Neurol. 9, 375–391 (2022). [PubMed: 35170874]

94. Dupont C. et al. , TRPV4 Antagonism Prevents Mechanically Induced Myotonia. Ann. Neurol. 88, 297–308 (2020). [PubMed: 32418267]

95. Sullivan JM et al. , Dominant mutations of the Notch ligand Jagged1 cause peripheral neuropathy. J. Clin. Invest. 130, 1506–1512 (2020). [PubMed: 32065591]

96. Zhou Y. et al. , Canonical WNT signaling components in vascular development and barrier formation. J. Clin. Invest. 124, 3825–3846 (2014). [PubMed: 25083995]

97. Zudaire E, Gambardella L, Kurcz C, Vermeren S, A computational tool for quantitative analysis of vascular networks. PLoS One 6, e27385 (2011).

98. Bhumbra GS, Beato M, Recurrent excitation between motoneurones propagates across segments and is purely glutamatergic. PLoS Biol. 16, e2003586 (2018).

99. Hochman S, Shreckengost J, Kimura H, Quevedo J, Presynaptic inhibition of primary afferents by depolarization: observations supporting nontraditional mechanisms. Ann. N. Y. Acad. Sci. 1198, 140–152 (2010). [PubMed: 20536928]

100. Ogata S, Ito S, Masuda T, Ohtsuki S, Efficient isolation of brain capillary from a single frozen mouse brain for protein expression analysis. J. Cereb. Blood Flow Metab. 41, 1026–1038 (2021). [PubMed: 32703112]

101. Ramos DM et al. , Age-dependent SMN expression in disease-relevant tissue and implications for SMA treatment. J. Clin. Invest. 129, 4817–4831 (2019). [PubMed: 31589162]

102. Aisenberg WH et al. , Multiubiquitination of TRPV4 reduces channel activity independent of surface localization. J. Biol. Chem. 298, 101826 (2022).

103. Sabbagh MF, Nathans J, A genome-wide view of the de-differentiation of central nervous system endothelial cells in culture. eLife 9, (2020).

104. Thorneloe KS, Cheung M, Holt DA, Willette RN, Properties of the TRPV4 agonist GSK1016790A and the TRPV4 antagonist GSK2193874. Physiol. Rev. 97, 1231–1232 (2017). [PubMed: 28794166]

105. Lawhorn BG, Brnardic EJ, Behm DJ, Recent advances in TRPV4 agonists and antagonists. Bioorg. Med. Chem. Lett. 30, 127022 (2020).

106. Yang J. et al. , PAC, an evolutionarily conserved membrane protein, is a proton-activated chloride channel. Science 364, 395–399 (2019). [PubMed: 31023925]

107. Wuest DM, Lee KH, Optimization of endothelial cell growth in a murine in vitro blood-brain barrier model. Biotechnol. J. 7, 409–417 (2012). [PubMed: 22095877]

108. Zhu Y. et al. , Ablation of NF1 function in neurons induces abnormal development of cerebral cortex and reactive g2liosis in the brain. Genes Dev. 15, 859–876 (2001). [PubMed: 11297510]

109. Alcantara Llaguno S. et al. , Cell-of-origin susceptibility to glioblastoma formation declines with neural lineage restriction. Nat. Neurosci. 22, 545–555 (2019). [PubMed: 30778149]

110. Pecho-Vrieseling E, Sigrist M, Yoshida Y, Jessell TM, Arber S, Specificity of sensory-motor connections encoded by Sema3e-Plxnd1 recognition. Nature 459, 842–846 (2009). [PubMed: 19421194]

111. Caggiano V. et al. , Midbrain circuits that set locomotor speed and gait selection. Nature 553, 455–460 (2018). [PubMed: 29342142]

112. Gorski JA et al. , Cortical excitatory neurons and glia, but not GABAergic neurons, are produced in the Emx1-expressing lineage. J. Neurosci. 22, 6309–6314 (2002). [PubMed: 12151506]
113. Hong YK, Lacefield CO, Rodgers CC, Bruno RM, Sensation, movement and learning in the absence of barrel cortex. Nature 561, 542–546 (2018). [PubMed: 30224746]
114. Kvitsiani D. et al. , Distinct behavioural and network correlates of two interneuron types in prefrontal cortex. Nature 498, 363–366 (2013). [PubMed: 23708967]
115. Hur JY et al. , The innate immunity protein IFITM3 modulates gamma-secretase in Alzheimer's disease. Nature 586, 735–740 (2020). [PubMed: 32879487]
116. Chen MJ, Yokomizo T, Zeigler BM, Dzierzak E, Speck NA, Runx1 is required for the endothelial to haematopoietic cell transition but not thereafter. Nature 457, 887–891 (2009). [PubMed: 19129762]
117. Fahs SA, Hille MT, Shi Q, Weiler H, Montgomery RR, A conditional knockout mouse model reveals endothelial cells as the principal and possibly exclusive source of plasma factor VIII. Blood 123, 3706–3713 (2014). [PubMed: 24705491]
118. Xu R. et al. , Targeting skeletal endothelium to ameliorate bone loss. Nat. Med. 24, 823–833 (2018). [PubMed: 29785024]
119. Kisanuki YY et al. , Tie2-Cre transgenic mice: a new model for endothelial cell-lineage analysis in vivo. Dev. Biol. 230, 230–242 (2001). [PubMed: 11161575]
120. Tian X. et al. , Vessel formation. De novo formation of a distinct coronary vascular population in neonatal heart. Science 345, 90–94 (2014). [PubMed: 24994653]
121. Tian L. et al. , Mutual regulation of tumour vessel normalization and immunostimulatory reprogramming. Nature 544, 250–254 (2017). [PubMed: 28371798]
122. Miniou P. et al. , Gene targeting restricted to mouse striated muscle lineage. Nucleic Acids Res. 27, e27 (1999). [PubMed: 10481039]
123. Knudsen NH et al. , Interleukin-13 drives metabolic conditioning of muscle to endurance exercise. Science 368, eaat3987 (2020).
124. Yamamoto M. et al. , A multifunctional reporter mouse line for Cre- and FLP-dependent lineage analysis. Genesis 47, 107–114 (2009). [PubMed: 19165827]
125. Holtwick R. et al. , Smooth muscle-selective deletion of guanylyl cyclase-A prevents the acute but not chronic effects of ANP on blood pressure. Proc. Natl. Acad. Sci. U. S. A. 99, 7142–7147 (2002). [PubMed: 11997476]
126. Ziegler SG et al. , Ectopic calcification in pseudoxanthoma elasticum responds to inhibition of tissue-nonspecific alkaline phosphatase. Sci. Transl. Med. 9, eaal1669 (2017).
127. Clausen BE, Burkhardt C, Reith W, Renkawitz R, Forster I, Conditional gene targeting in macrophages and granulocytes using LysMcre mice. Transgenic Res. 8, 265–277 (1999). [PubMed: 10621974]
128. McCauley ME et al. , C9orf72 in myeloid cells suppresses STING-induced inflammation. Nature 585, 96–101 (2020). [PubMed: 32814898]
129. Garcia AD, Doan NB, Imura T, Bush TG, Sofroniew MV, GFAP-expressing progenitors are the principal source of constitutive neurogenesis in adult mouse forebrain. Nat. Neurosci. 7, 1233–1241 (2004). [PubMed: 15494728]
130. Qian H. et al. , Reversing a model of Parkinson's disease with in situ converted nigral neurons. Nature 582, 550–556 (2020). [PubMed: 32581380]
131. Lappe-Siefke C. et al. , Disruption of Cnp1 uncouples oligodendroglial functions in axonal support and myelination. Nat. Genet. 33, 366–374 (2003). [PubMed: 12590258]
132. Funfschilling U. et al. , Glycolytic oligodendrocytes maintain myelin and long-term axonal integrity. Nature 485, 517–521 (2012). [PubMed: 22622581]
133. Ito Y. et al. , RIPK1 mediates axonal degeneration by promoting inflammation and necroptosis in ALS. Science 353, 603–608 (2016). [PubMed: 27493188]
134. Jaegle M. et al. , The POU proteins Brn-2 and Oct-6 share important functions in Schwann cell development. Genes Dev. 17, 1380–1391 (2003). [PubMed: 12782656]

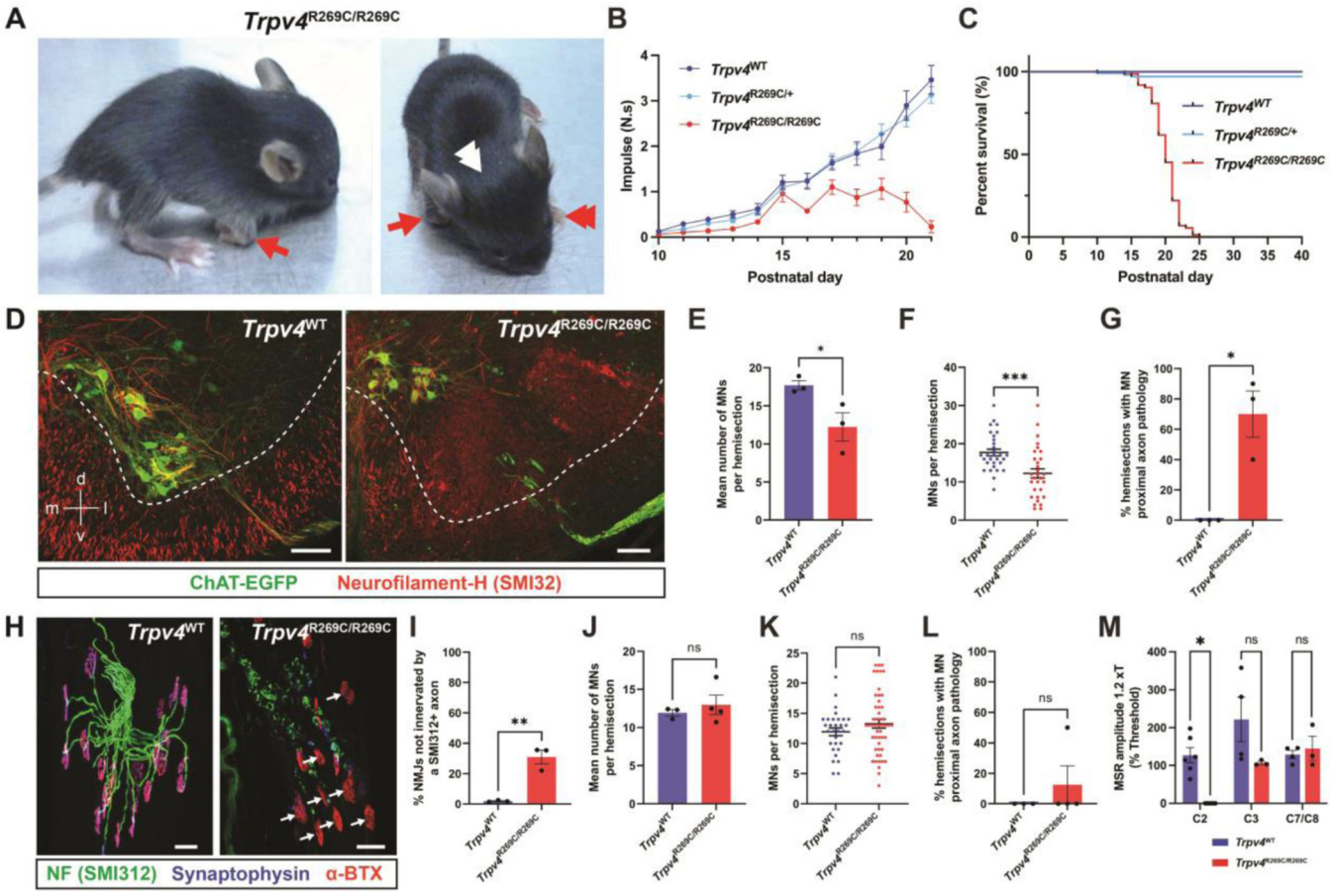

Fig. 1. *Trpv4*$^{R269C/R269C}$ mice exhibit marked neurological phenotypes.

(**A**) Representative photographs of a symptomatic phase *Trpv4*$^{R269C/R269C}$ mouse (*Stage B*) exhibiting asymmetric forelimb paralysis (red arrow and red arrowheads) and an inability to maintain upright head posture (white arrowheads). (**B**, **C**) Forelimb hang test motor performance (B) and survival curve (C) of *Trpv4*$^{R269C/R269C}$, *Trpv4*$^{R269C/+}$, and *Trpv4*^{WT} mice (B, n=22–43 mice/genotype; C, n=50–101 mice/genotype). Hang impulse (N.s) reflects the force exerted by the mouse to oppose gravity. (**D**) Confocal images of the C1 spinal cord ventral horn of *Trpv4*^{WT} and symptomatic phase *Trpv4*$^{R269C/R269C}$ (*Stage C*) mice. The dashed white lines indicate the grey matter boundary. Scale bar = 100 μm. Unmerged images are shown in fig. S3. (**E**, **F**) Mean number of MNs per C1 spinal cord hemisection, based on assessments of the mean number per mouse (E; n=3 mice/genotype) and per hemisection (F; n=30 hemisections/genotype). All *Trpv4*$^{R269C/R269C}$ mice were in symptomatic phase *Stage C*. (**G**) Percent of C1 spinal cord hemisections exhibiting signs of MN proximal axon pathology (axonal swelling and fragmentation; see also fig. S3; n=3 mice/genotype). *Trpv4*$^{R269C/R269C}$ mice were in symptomatic phase *Stage C*. (**H**, **I**) Confocal images (H) and quantification (I) of NMJ denervation (arrows in H) in the semispinalis capitis muscle, a neck muscle innervated by MNs at the C1–3 spinal cord levels (n=3 mice/genotype, >1000 NMJs analyzed per animal). Scale bars = 25 μm. (**J**-**L**) Assessments of MN numbers (J, K) and proximal axon pathology (L) in C1 spinal cord sections of symptomatic phase *Trpv4*$^{R269C/R269C}$ mice at *Stage B*. Shown are the mean number of MNs per C1 spinal cord

hemisection, based on assessments of the mean number per mouse (J, n=3–4 mice/genotype) and per hemisection (K, n=30–50 hemisections/genotype), and the percent of C1 spinal cord hemisections exhibiting signs of MN proximal axon pathology (L, n=3–4 mice/genotype). (**M**) Quantification of monosynaptic sensory-motor reflex (MSR) amplitude at the C2, C3, and C7-C8 spinal cord levels of *Trpv4*$^{R269C/R269C}$ mice at *Stage B* (n=3–6 mice/genotype). BTX, α-bungarotoxin, C1–3, cervical spinal cord levels 1–3, NF, neurofilament-H. Plots show mean ± SEM; (E, F, I, J, K) unpaired two-sided *t*-test, (G, L) unpaired two-sided *t*-test with Welch's correction, (M) two-way ANOVA, Tukey's multiple comparison test; ns, not significant, $*P \leq 0.05$, $**P < 0.01$, $***P < 0.001$.

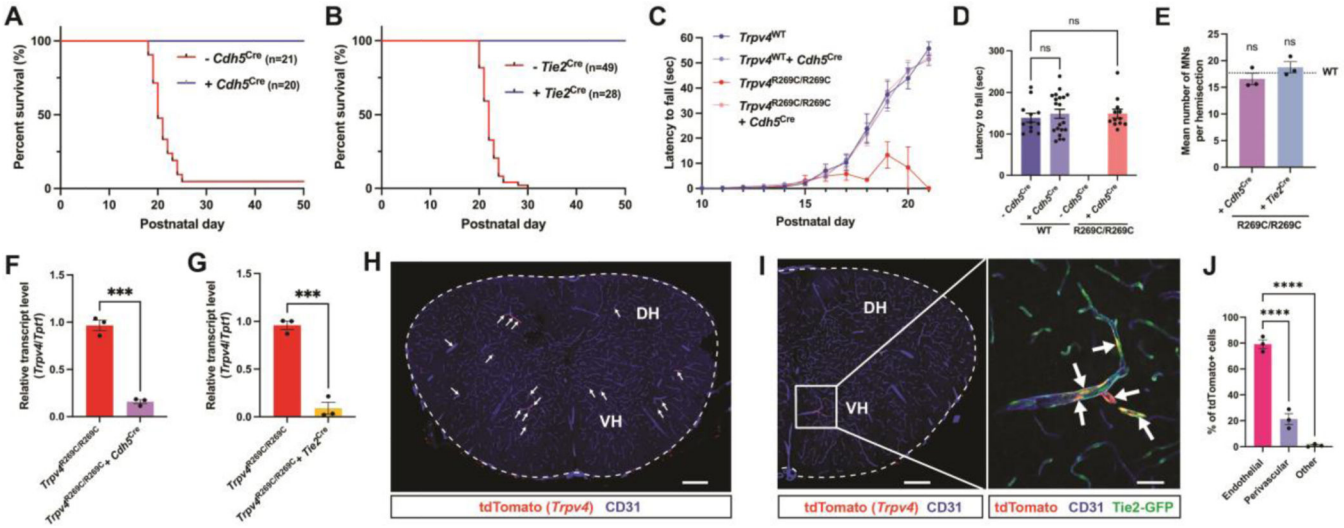

Fig. 2. Genetic deletion of mutant TRPV4 from endothelial cells rescues *Trpv4*$^{R269C/R269C}$ mice.

(**A**) Survival curves of *Trpv4*$^{R269C/R269C}$ and *Trpv4*$^{R269C/R269C}$; *Cdh5*^{Cre} littermate mice. (**B**) Survival curves of *Trpv4*$^{R269C/R269C}$ and *Trpv4*$^{R269C/R269C}$; *Tie2*^{Cre} littermate mice. (**C, D**) Motor performance of *Trpv4*$^{R269C/R269C}$ mice expressing *Cdh5*^{Cre} in the horizontal balance test (C; n=10–25 mice/genotype) and accelerating rotarod assay (D; mice aged 2–6 months, n=12–20 mice/genotype). (**E**) Mean number of MNs per C1 spinal cord hemisection in *Trpv4*$^{R269C/R269C}$ mice expressing *Cdh5*^{Cre} or *Tie2*^{Cre} (n=3 mice/genotype; n=30 hemisections/genotype). Statistical comparisons are to WT mice (dashed horizontal line, from Fig. 1E). (**F**, **G**) RT-qPCR analysis demonstrating knockdown of *Trpv4* transcript in the isolated forebrain vasculature of *Trpv4*$^{R269C/R269C}$ mice with endothelial cell-specific Cre expression (F, +*Cdh5*^{Cre}; G, +*Tie2*^{Cre}; n=3 mice/genotype). (**H**, **I**) Representative confocal images showing the expression of the tdTomato reporter in NVECs (arrows) in C1 spinal cord, including within the ventral horn (I). Unmerged images are shown in fig. S9. Scale bars = 200 μm (H, I left), 50 μm (I right). (**J**) Quantification of the cell types in C1 spinal cord containing tdTomato reporter signal. DH, dorsal horn; VH, ventral horn. Plots show mean ± SEM; (D, E) one-way ANOVA, (F, G) unpaired two-sided *t*-test, (J) one-way ANOVA, Dunnett's multiple comparison test; ns, not significant, ***$P < 0.001$. ****$P < 0.0001$.

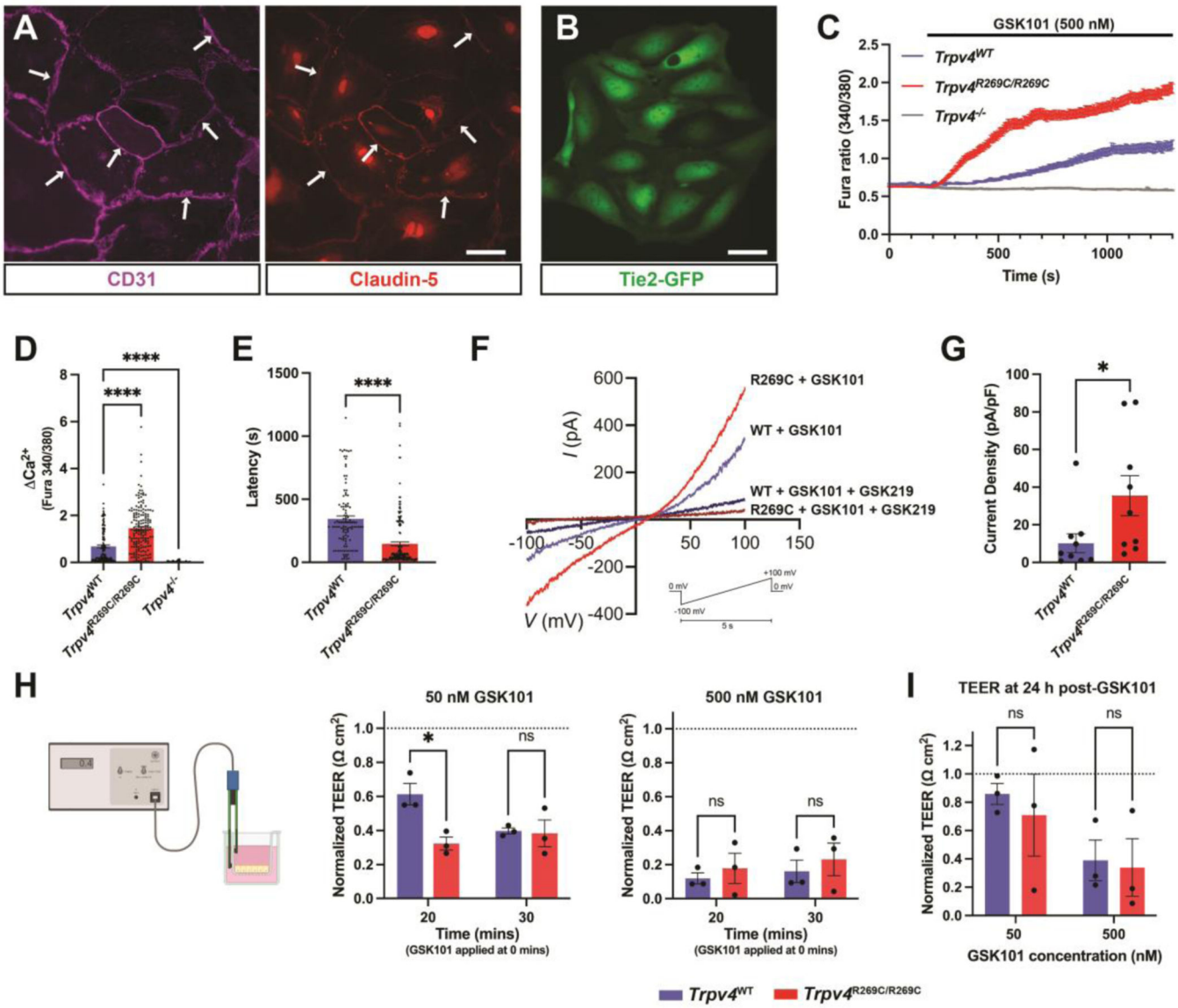

Fig. 3. Mutant TRPV4 channels in NVECs exhibit a gain-of-function in channel activity.

(**A**) Representative immunofluorescence staining for CD31 (left) and Claudin-5 (right) in NVECs cultured from the brainstem and cervical spinal cord. White arrows indicate junctional complexes between adjacent cells. Scale bar = 50 μm. (B) Epifluorescence image of cultured NVECs showing GFP expression from the Tie2-GFP allele. Scale bar = 20 μm. (**C**) Shown are changes in the Fura-2 ratio (emission at 340/380 nm), an indicator of alterations in cytosolic free calcium (Ca^{2+}), evoked by application of the TRPV4-specific agonist GSK101 to NVECs isolated from *Trpv4*^{WT}, *Trpv4*$^{R269C/R269C}$, and *Trpv4*$^{-/-}$ mice (n=112–172 cells/genotype, n=4 NVEC isolations for *Trpv4*^{WT} and *Trpv4*$^{R269C/R269C}$, n=2 isolations for *Trpv4*$^{-/-}$). (**D**) Magnitude of the calcium responses for the same NVEC genotypes as in C. Changes in cytosolic free calcium (ΔCa^{2+}) following GSK101 application were calculated by subtracting the basal Fura-2 ratio (mean over 175 seconds immediately pre-GSK101 application) for each cell from the maximum value recorded over 1160 seconds

post-GSK101 application. (**E**) Calcium response latency for cultured NVECs from *Trpv4*^{WT} and *Trpv4*$^{R269C/R269C}$ mice. (**F**) Representative current-voltage relationship of whole-cell TRPV4 currents in response to a voltage ramp (see inset) recorded from cultured *Trpv4*^{WT} and *Trpv4*$^{R269C/R269C}$ NVECs in the presence of GSK101 (5 μM) and after perfusion of the TRPV4-specific antagonist GSK219 (6.67 μM). (**G**) Quantification of current density in whole-cell patch clamp recordings from cultured *Trpv4*^{WT} and *Trpv4*$^{R269C/R269C}$ NVECs following application of GSK101 (5 μM) (n= 9–10 cells/genotype, n=3 NVEC isolations for *Trpv4*^{WT} and *Trpv4*$^{R269C/R269C}$). (**H**) (left) Illustration of setup for TEER measurements (Ω cm^2) across confluent monolayers of cultured NVECs from *Trpv4*$^{R269C/R269C}$ and *Trpv4*^{WT} mice. (center, right) Normalized TEER at 20 and 30 minutes following application of GSK101 (at 0 mins), (**I**) Normalized TEER at 24 hrs post-agonist application. Measurements collected following GSK101 application were first normalized to baseline TEER, to assess fold changes, and then normalized to the mean TEER of vehicle-treated wells of the same genotype/time point, to account for non-specific effects of drug addition (for example, mechanical disturbance) (n=3 NVEC isolations for *Trpv4*^{WT} and *Trpv4*$^{R269C/R269C}$). Plots show mean ± SEM; (D) Kruskal-Wallis test, Dunn's multiple comparison test, (E) unpaired two-sided *t*-test with Welch's correction, (G) unpaired two-sided *t*-test, (H, I) two-way ANOVA, Tukey's multiple comparison test; ns, not significant, $*P \leq 0.05$, $****P < 0.0001$. The schematic of the TEER experiment (H, left) was created using BioRender.com.

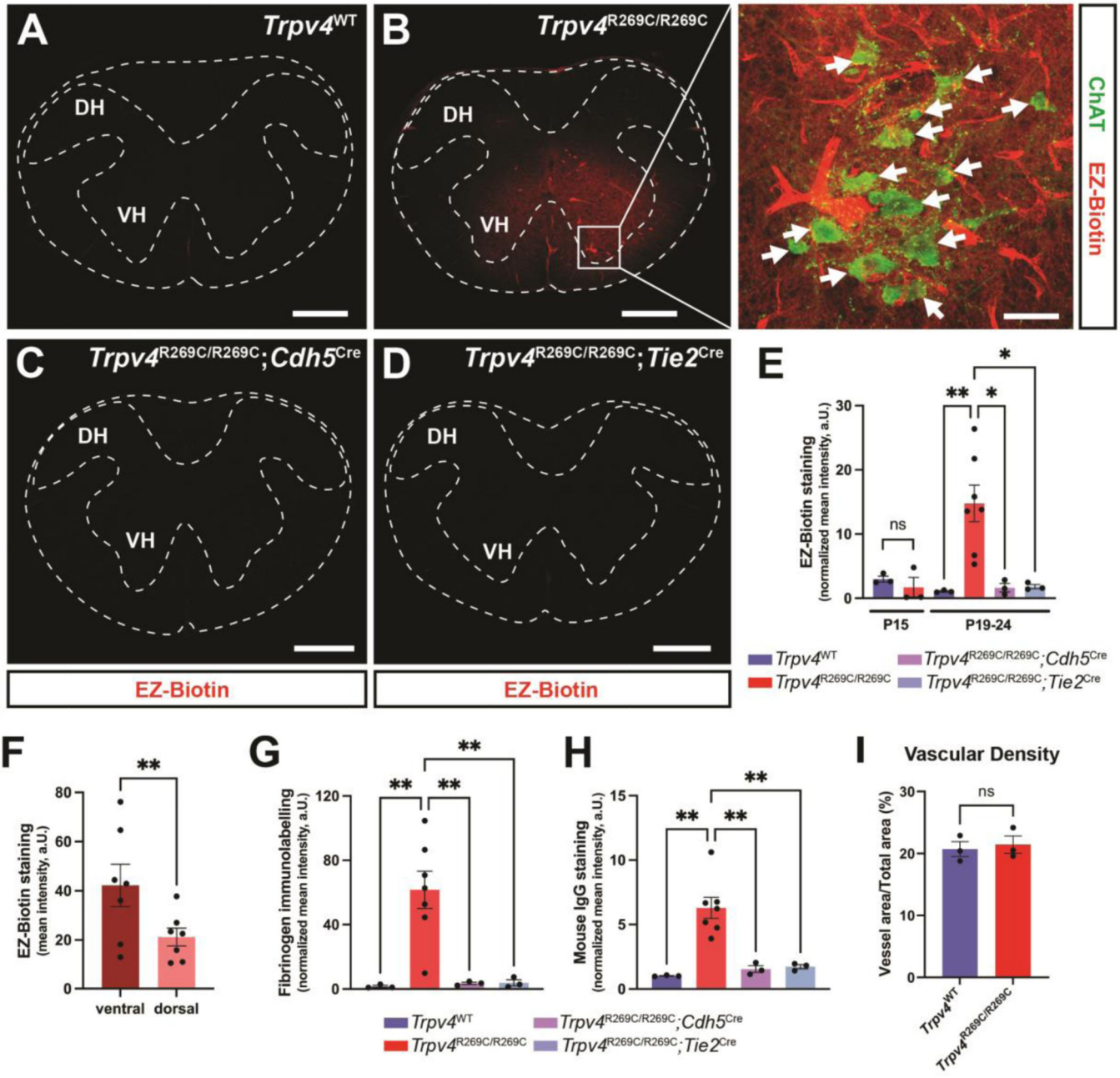

Fig. 4. Mutant TRPV4 expression disrupts BSCB integrity.

(**A-D**) Representative images of EZ-Biotin staining in cross sections of C1 spinal cord for *Trpv4*^{WT} (A), *Trpv4*$^{R269C/R269C}$ (*Stage B*) (B), *Trpv4*$^{R269C/R269C}$;*Cdh5*^{Cre} (C), and *Trpv4*$^{R269C/R269C}$;*Tie2*^{Cre} (D) mice. The inset for B shows EZ-Biotin staining (red) adjacent to motor neuron somata (green). Scale bars = 400 μm (A-D), 50 μm (inset for B). (**E**) Quantification of normalized EZ-Biotin staining intensity in C1 spinal cord cross sections for the genotypes in A-D. Staining intensities (a.U.) were normalized to the mean for one of the *Trpv4*^{WT} mice. (**F**) Quantification of EZ-Biotin staining intensity in the dorsal and ventral halves of C1 spinal cord of *Trpv4*$^{R269C/R269C}$ (*Stage B*) mice. (**G**, **H**) Quantification

of fibrinogen (G) and mouse IgG (H) staining intensity in C1 spinal cord (n=3–7 mice/genotype, n=8–11 sections/mouse) for the genotypes in A-D. (**I**) Quantification of the vascular density of the C1 spinal cord ventral horn of presymptomatic *Trpv4*$^{R269C/R269C}$ mice at P15 (n=3 mice/genotype; n=7–10 hemisections/mouse) compared to *Trpv4*^{WT} littermates. DH, dorsal horn, VH, ventral horn. Plots show mean ± SEM; (E, G, H) one-way ANOVA, Dunnett's multiple comparison test, (F) paired two-sided *t*-test, (I) unpaired two-sided *t*-test; ns, not significant, $*P \leq 0.05$ $**P < 0.01$.

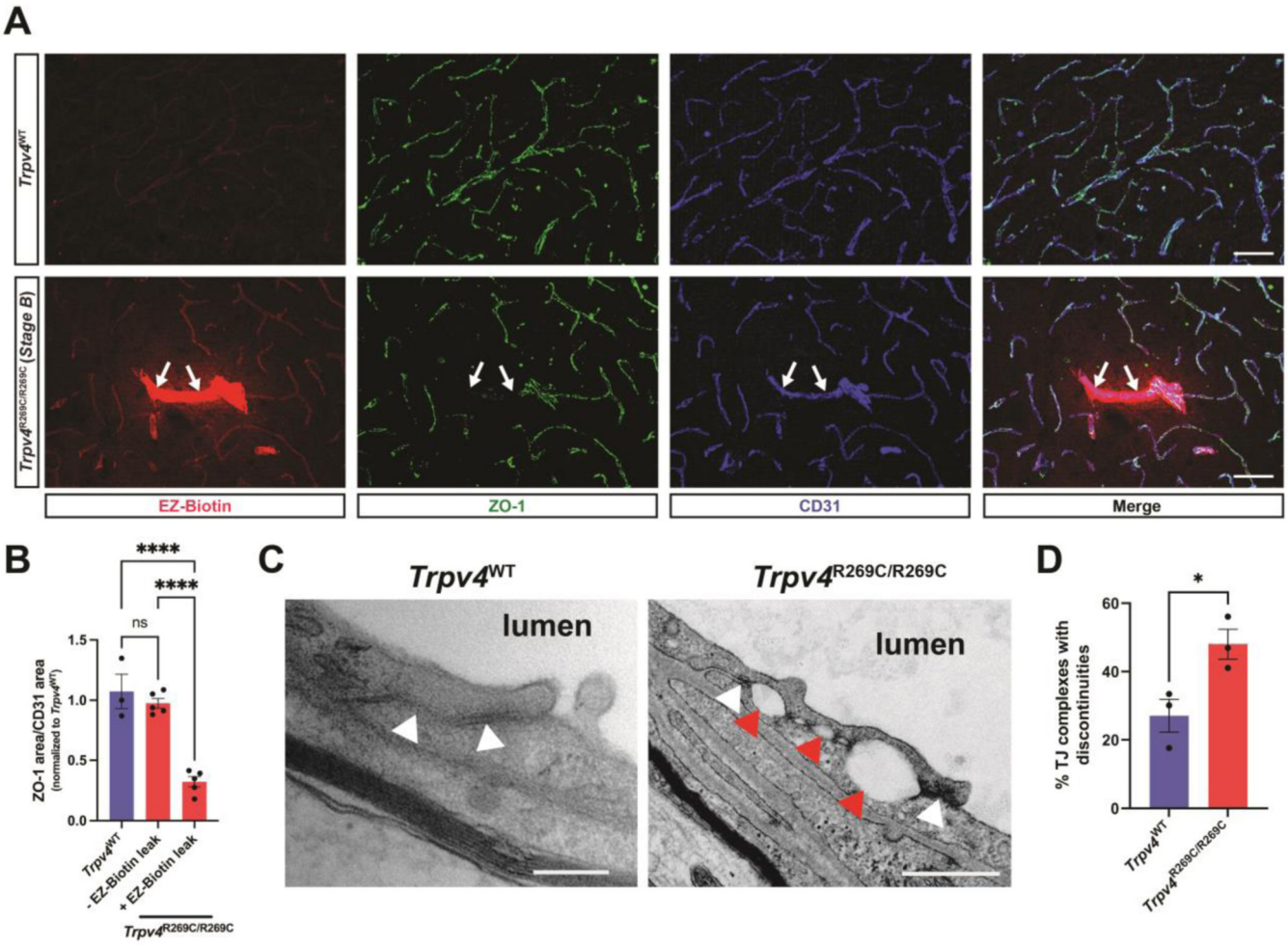

Fig. 5. Symptomatic TRPV4 mutant mice exhibit disruptions of NVEC tight junction complexes.

(**A, B**) Representative structured illumination microscopy images (A) and quantification (B) of the ratio of ZO-1 and CD31 staining area in cross sections of C1 spinal cord of *Trpv4*^{WT} and *Trpv4*$^{R269C/R269C}$ (*Stage B*) mice (n=3–5 mice/genotype; n=9 sections/mouse). Analysis of symptomatic mutant mice was performed on vessels in which EZ-Biotin leak was either absent (- EZ-Biotin leak) or present (+ EZ-Biotin leak). Arrows indicate regions of ZO-1 loss. Scale bars = 50 μm. (**C**) Transmission electron microscopy images of upper cervical spinal cord NVECs revealed discontinuities (red arrowheads) of tight junction complexes (white arrowheads). Scale bars = 500 nm. (**D**) Quantification of the proportion of tight junction complexes exhibiting discontinuities (n=3 mice/genotype; n= 38–107 tight junction complexes/mouse). Plots show mean ± SEM; (B) one-way ANOVA, Tukey's multiple comparison test, (D) unpaired two-sided *t*-test; ns, not significant, *$P \leq 0.05$, ****$P < 0.0001$.

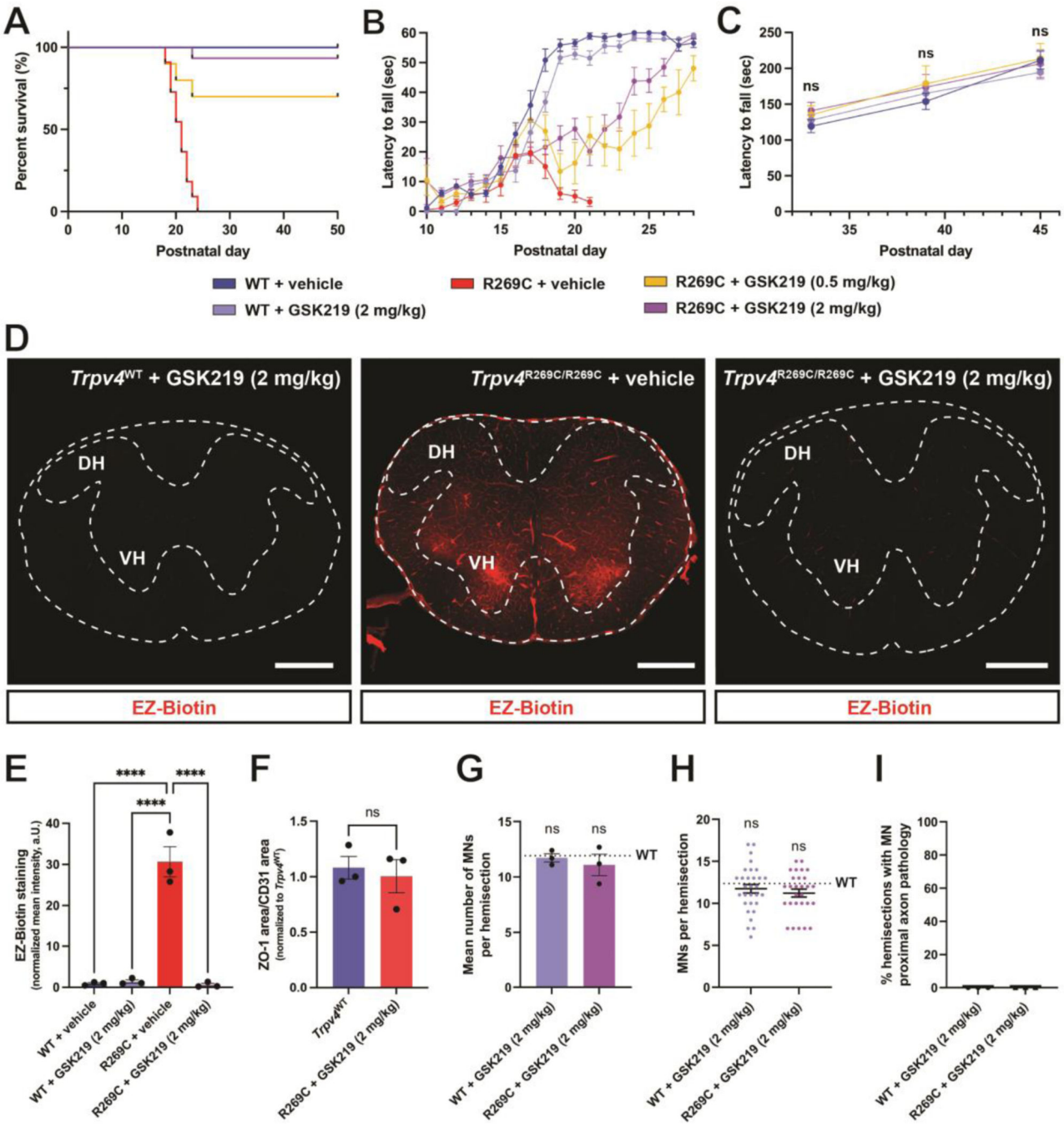

Fig. 6. Systemic administration of a TRPV4-specific antagonist rescues symptomatic *Trpv4*$^{R269C/R269C}$ mice.

(A-C) Survival (A) and motor performance in the horizontal balance test (B; n=10–15 mice/genotype) and accelerating rotarod assay (C; n=7–14 mice/genotype) of GSK219- (*Trpv4*^{WT} + 2 mg/kg GSK219, *Trpv4*$^{R269C/R269C}$ + 0.5 mg/kg GSK219, *Trpv4*$^{R269C/R269C}$ + 2 mg/kg GSK219) and vehicle-treated mice (*Trpv4*^{WT} + vehicle, *Trpv4*$^{R269C/R269C}$ + vehicle). (**D**, **E**) Representative images (D) and quantification (E) of EZ-Biotin staining in C1 spinal cord of GSK219- and vehicle-treated mice (n=3 mice/cohort, n=5 sections/

mouse; R269C + vehicle cohort, P20–22, other cohorts, P50–60). Scale bars = 400 μm. (**F**) Quantification of the ratio of ZO-1 and CD31 staining area in C1 spinal cord of GSK219-treated *Trpv4*$^{R269C/R269C}$ and age-matched *Trpv4*^{WT} mice (n=3 mice/genotype). (**G-I**) Assessments of MN numbers (G, H) and proximal axon pathology (I) in C1 spinal cord sections of GSK219- and vehicle-treated mice. Shown are the mean number of MNs per C1 spinal cord hemisection, based on assessments of the mean number per mouse (G, n=3 mice/cohort) and per hemisection (H, n= 8–16 hemisections/mouse), and the percent of C1 spinal cord hemisections exhibiting signs of MN proximal axon pathology (I, n=3 mice/cohort; 8–16 hemisections/mouse). Statistical comparisons are to WT mice (dashed horizontal line). DH, dorsal horn; VH, ventral horn. (D). Plots show mean ± SEM; (C) two-way ANOVA, (E, G-H) one-way ANOVA, Dunnett's multiple comparison test, (F) unpaired two-sided *t*-test; ns, not significant, ****$P < 0.0001$.